Available online at www.sciencedirect.com
ScienceDirect
Journal of Power Sources 170 (2007) 13–19
JOURNAL OF POWER SOURCES
www.elsevier.com/locate/jpowsour

Facile fabrication and electrocatalytic activity of $Pt_{0.9}Pd_{0.1}$ alloy film catalysts

Yanhui Xu, Xiangqin Lin *

Department of Chemistry, University of Science and Technology of China, Hefei 230026, PR China

Received 14 December 2006; received in revised form 9 March 2007; accepted 9 March 2007
Available online 12 April 2007

Abstract

A nano-thickness porous $Pt_{0.9}Pd_{0.1}$ alloy film with a greatly enhanced surface area were firstly synthesized at a glassy carbon electrode (GCE) using a facile cyclic voltammetry (CV) method. The atomic ratio of the alloy can be controlled by controlling the composition of the electrodeposition solution. We found that small amount of alloying Pd is an excellent catalytically enhancing agent for the Pt catalyst, and 10% Pd is the optimal. The structures of the $Pt_{0.9}Pd_{0.1}$ alloy film were characterized by FE-SEM, XPS, XRD and electrochemical techniques. It was found that the $Pt_{0.9}Pd_{0.1}$ film was in nanoporous structure and consisted of crystallites of 10.1 nm on average, leading to the modified electrode ($Pt_{0.9}Pd_{0.1}$/GCE) has an effective surface area as large as 790 times that of a corresponding bare Pt disk electrode. The $Pt_{0.9}Pd_{0.1}$/GCE exhibited significantly higher stability and catalytic activity for both of the methanol electro-oxidation reaction (MOR) and the oxygen electro-reduction reaction (ORR) than the correspondingly electrodeposited Pt modified GCE. The advantage can be attributed to the CV-prepared nano-porous structure on the electrode surface. This method and the prepared electrode can be expected to have promising applications in biosensors and fuel cells, etc.

Keywords: Alloy film; Electrodeposition; Catalyst; Oxygen electro-reduction; Methanol electro-oxidation

1. Introduction

Many efforts have paid on the development of techniques to produce Pt catalysts with a high surface area to achieve high catalytic performance and utilization efficiency. The Pt nanoparticles (<10 nm) with enlarged surface area have been prepared with different methods [1,2]. Many researchers have shown a considerable interest in using nanostructured Pt film for improving the Pt catalytic activity, which can be prepared based on liquid crystal templates [3–5], hydrothermal-assisted seed growth [6] and electrochemical dealloying [7–9]. The liquid crystal template techniques have the advantage of control over the size of the porous structure, but are generally difficult and time-consuming to implement. The hydrothermal-assisted seed method is also time-consuming.

Nanostructured Pt and Pt-based alloy is of considerable interest as it is known to be one of the most important catalysts for many chemical reactions, for example, selective electrocatalytic hydrogenation of NO_3^- to N_2 [10], catalytic oxidation of SO_2 to SO_3 [11], production of hydrogen from cyclohexane [12], biosensors [13–15] and especially the oxygen reduction reaction (ORR) and methanol oxidation reaction (MOR) in fuel cells [16–20]. Because of the high overpotential for the typical fuel operating conditions (at least 0.3–0.4 V), Pt alloy catalysts with various transition metals were employed to increase the catalytic activity and decrease the cost. Investigations have shown that some Pt-based catalysts, such as Pt–M [21–26] (where M = Co, Ni, Fe, V, Mn, and Cr), exhibited an enhanced electrocatalytic activity for the ORR compared with pure Pt alone. Electrochemical dealloying Pt with Zn [7] and Cu [9] have been reported, which shows the advantage of enlarging effective surface area, enhancing the catalytic activity and stability of the catalyst by using constant potential dealloying. However, how to select the critical potential for alloy dissolution to achieve optimum catalytic activity is difficult. Although some sort of PtPd alloy nanoparticles has been reported, such as prepared by water-in-oil technique [27], and by normal wet impregnation technique and flame aerosol synthesis [28], however, these techniques were complex and time-consuming. Nano-thickness porous PtPd alloy film has not been synthesized for investigation.

* Corresponding author. Tel.: +86 551 3606646; fax: +86 551 3601592.
E-mail address: xqlin@ustc.edu.cn (X. Lin).

0378-7753/$ – see front matter © 2007 Elsevier B.V. All rights reserved.
doi:10.1016/j.jpowsour.2007.03.064

MOR has been thoroughly investigated for methanol is an important liquid fuel for fuel cells. Although Pt- and Pd-based alloys are important catalysts for fuel cell applications, however, how to improve the utilization and efficiency of the Pt-based anodic materials is still a challenge [29]. On the other hand, ORR is a reaction of prime importance in many industrial, environmental [30–32], and electrochemical applications like biosensor [33] and fuel cells [25,34]. The improvement in the ORR electrocatalysis on Pt alloy catalysts has been explained by several factors such as electronic and structural effects [35–37].

In this work, we report a nanoporous $Pt_{0.9}Pd_{0.1}$ alloy film with a greatly enhanced surface area electrodeposited at a glassy carbon electrode (GCE) surface by multi-cycle cyclic voltammetry (CV) method. The preparation was carried out at room temperature. The method is simple, cost-effective, and adaptable. This homogeneous nanostructured $Pt_{0.9}Pd_{0.1}$ alloy film exhibited high stability and remarkable catalytic activity for MOR and ORR with promising applications in fuel cells and biosensors.

2. Experimental

2.1. Chemicals

H_2PtCl_6, $PdCl_2$, H_2SO_4 and CH_3OH were obtained from Chemical Reagent Company of Shanghai (Shanghai, China). All chemicals used were of analytical grade. Doubly distilled water was used. High purity nitrogen and dioxygen (99.999%, Shanghai Pujiang Special Gas Corporation, China) were used.

2.2. Instruments

Cyclic voltammetry (CV) measurements were performed with a CHI 660A electrochemical workstation (CHI, Shanghai, China). A one-compartment three-electrode cell system was used, which consisted of a testing electrode, a platinum wire auxiliary electrode, and a saturated calomel reference electrode (SCE) placed in a glass frit for solution separation. All potentials in this work were referred to the SCE. A glassy carbon disk electrode (GCE, $\Phi = 4$ mm, formal surface area = 0.126 cm^2) and a Pt disc electrode ($\Phi = 4$ mm) (Lan-Like HCET company, TianJing, China) were used as the basal electrodes for fabrication. All experiments were carried out at room temperature.

X-ray photoelectron spectroscopy (XPS) was performed on ESCALAB MKII spectrometer (VG Co., UK), using Mg Kα radiation (1253.6 eV) at a pressure of 2.0×10^{-10} mbar. The peak positions were internally referenced to the C 1s peak at 284.6 eV.

X-ray diffraction (XRD) was recorded on a X′pert Philips diffractometer using Cu Kα radiation (λ = 1.54178 A) with a Ni filter.

Field emission scanning electron microscope (FE-SEM) image was obtained on a JSM-6700F field emission scanning electron microanalyser (JEOL, Japan) for characterizing the morphology of the catalysts, operating at 5 kV.

2.3. Experimental details

Prior to each experiment, the bare GCE or PDE was polished to a mirror finish using 0.3 and 0.05 μm alumina power, ultrasonically cleaned in ethanol and water bath twice for 5 min and dried under nitrogen stream.

The electrodeposition of Pt, Pd and Pt–Pd alloy was all accomplished with potential cycling between 1.2 and −0.24 V at a scan rate of 100 mV s^{-1} for 120 cycles in a freshly prepared solution.

The electrocatalytic reduction of oxygen was carried out in an oxygen-saturated 0.5 M H_2SO_4 solution. The electrocatalytic oxidation of methanol was carried out in a 1.0 M H_2SO_4 solution containing 1.0 M methanol and the chronoamperometry measurements were made in the solution with a potential jump from 0.0 to 0.4 V. The electrolysis current of MOR was normalized by the platinum loading (L_{Pt}, mg) to calculate the mass current density (mA mg^{-1}). The real surface area of the deposited Pt and $Pt_{0.9}Pd_{0.1}$ alloy film on GCE were determined from the charge associated with the hydrogen adsorption and desorption processes in 1.0 M H_2SO_4 solution at a scan rate of 100 mV s^{-1} using a conversion factor of 0.21 mC cm^{-2} [38,39].

3. Results and discussion

The electrodeposited Pt/GCE, Pd/GCE and $Pt_{0.9}Pd_{0.1}$/GCE were prepared in 0.5 M H_2SO_4 solution containing 6.0 mM H_2PtCl_6, 0.8 mM $PdCl_2$, and 6.0 mM H_2PtCl_6 + 0.8 mM $PdCl_2$, respectively. Typical FE-SEM images of them are presented in Fig. 1. It can be seen that the electrodeposited Pt is cone-shaped nanocrystal, the electrodeposited Pd is 2D trigeminal star nanocrystal, which is novel and has not been shown in the literature, as the best of our knowledge. It was evident from Fig. 1C and D that the PtPd alloy electrodeposited on GCE was a uniform and nanoporous film. To our knowledge, few PtPd alloy film has been reported.

Fig. 2 shows the Pt 4f (A) and Pd 3d (B) spectra of these electrodes. Two characteristic binding energies of 71.25 and 74.60 eV for the electrodeposited Pt correspond to Pt $4f_{7/2}$ and Pt $4f_{5/2}$, respectively, indicating the existence of Pt metal (curve a). The binding energies of 335.38 and 340.64 eV for the electrodeposited Pd correspond to Pd $3d_{5/2}$ and Pd $3d_{3/2}$, respectively, indicating the existence of Pd metal (curve b). Both of the Pt 4f and Pd 3d bands appearing for the Pt/Pd alloy film (curve c) indicate the codeposition of Pt and Pd. However, obvious shifts of the peak positions can be observed, as summarized in Table 1, which can be related to the perturbed electronic interaction between Pt and Pd atomic orbit and in turn to its alloy formation [40,41].

Table 1
The peak shifts in XPS of $Pt_{0.9}Pd_{0.1}$ alloy film

Electrode	Pt(0) (eV)		Pd(0) (eV)	
	$4f_{7/2}$	$4f_{5/2}$	$3d_{5/2}$	$3d_{3/2}$
Pt/GCE	71.25	74.60	–	–
Pd/GCE	–	–	335.38	340.64
$Pt_{0.9}Pd_{0.1}$/GCE	71.11	74.47	335.97	341.26

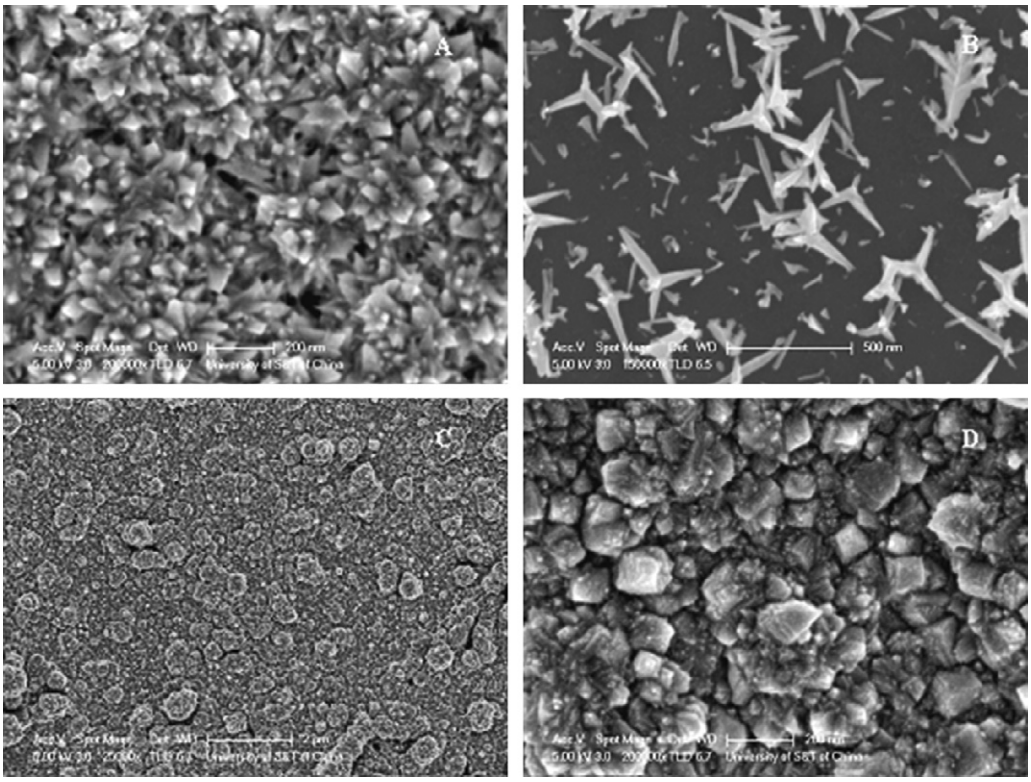

Fig. 1. FE-SEM image of the electrodeposited Pt (A), Pd (B) and $Pt_{0.9}Pd_{0.1}$ alloy film. (C) On the glassy carbon substrate. (D) A magnification of (C).

Furthermore, from XPS analyses, the atomic ratio of Pt:Pd for the electrodeposited alloy film can be estimated as be 9:1. The atomic ratio of Pt:Pd, n_1/n_2, was calculated form the integral values of the XPS peak area (I) and sensitivity factors (S) of Pt and Pd, $n_1/n_2 = (I_1/S_1)/(I_2/S_2)$,. The sensitivity factors are for Pt(0)$4f_{7/2}$ and Pd(0)$3d_{5/2}$.

As can be seen, the Pt:Pd ratio of the electrodeposition solution, $[H_2PtCl_6]/[PdCl_2]$, was 7.5:1, which is roughly consistent with the atom ratio, 9:1, in the alloy. We examined several solutions in different Pt:Pd ratio, similar result was obtained, as shown in Table 2. This suggested that the atomic ratio of PtPd alloy prepared by our method can thus be approximately controlled by controlling the concentration ratio in the electrodeposition concentration over a range. This is important since then we can conveniently and quantitatively control the composition of the alloy, subsequently tune the catalytic activity to obtain its optimum.

Fig. 3 shows the XRD patterns of the electrodeposited Pt (a) and $Pt_{0.9}Pd_{0.1}$ alloy (b). Curve a shows five diffraction peaks of (1 1 1), (2 0 0), (2 2 0), (3 1 1) and (2 2 2) at 2θ values of 39.9°, 46.4°, 67.7°, 81.5°and 86.0°, respectively. These peaks demonstrate the presence of face-centered cubic (fcc) Pt crystalite. For the $Pt_{0.9}Pd_{0.1}$ alloy, curve b presents diffraction patterns similar to those on curve a except the 2θ peak positions. All the five peak positions are shifted to higher degrees, which can be seen clearly in the inset of this figure, demonstrating the formation of single-phase $Pt_{0.9}Pd_{0.1}$ alloy. The lattice parameter of peak (2 2 0) was calculated for the $Pt_{0.9}Pd_{0.1}$ as 1.38356 Å, which is little larger than that for the pure Pt catalyst (1.38145 Å) due to Pd alloying [42,43].

Table 2
Comparison between the composition of the electrodeposition concentration and Pt/Pd atomic ratio in the alloy from XPS analysis

Deposition solution	Concentration (mM)		Atomic ratio in the alloy (Pt/Pd)
	H_2PtCl_2	$PdCl_2$	
1	1.0	3.0	$Pt_{0.23}/Pd_{0.77}$
2	2.0	2.0	$Pt_{0.51}/Pd_{0.49}$
3	3.0	2.0	$Pt_{0.57}/Pd_{0.43}$
4	6.0	0.8	$Pt_{0.50}/Pd_{0.10}$

An average nanocrystallite size of 11.7 and 10.1 nm for the electrodeposited Pt and $Pt_{0.9}Pd_{0.1}$respectively can be calculated using the Debye–Scherrer equation (Eq (1)), where the d is average particle size, $\lambda_{K\alpha}$ the wavelength of X-ray, θ_B the isolated angle of (2 2 0) peak, and $B_{(2\theta)}$ is the peak broadening:

$$d = \frac{0.9\lambda_{K\alpha}}{B_{(2\theta)}\cos\theta_B} \quad (1)$$

The total surface area of corresponding catalyst can be estimated from the XRD peaks analysis using Eq. (2) [44]:

$$S = \frac{6000}{\rho d} \quad (2)$$

where S is the surface area ($m^2\,g^{-1}$), d the average particle size (nm) from XRD analysis, and ρ the density ($\rho_{Pt} = 21.4\,g\,cm^{-3}$, $\rho_{Pd} = 12.0\,g\,cm^{-3}$ and the $Pt_{0.9}/Pd_{0.1}$ alloy density = $20.8\,g\,cm^{-3}$ from the calculation: $\rho_{alloy} = W_{Pt}\% \times \rho_{Pt} + W_{Pd}\% \times \rho_{Pd}$, where $W\%$ means weight percent).

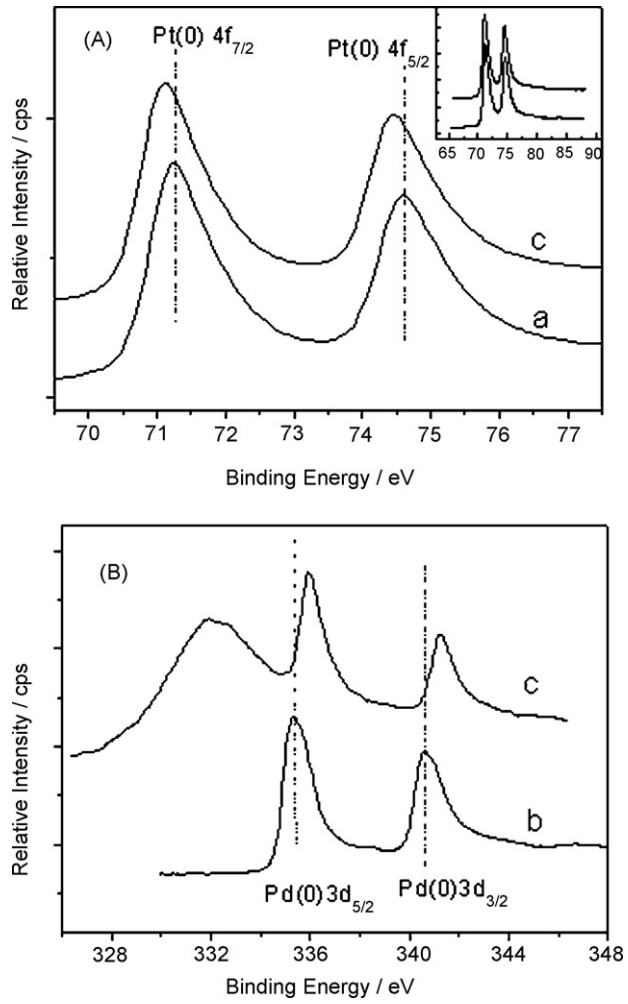

Fig. 2. XPS spectra of Pt 4f (A) Pd 3d (B) on Pt/GCE (a) Pd/GCE (b) and $Pt_{0.9}Pd_{0.1}$/GCE (c).

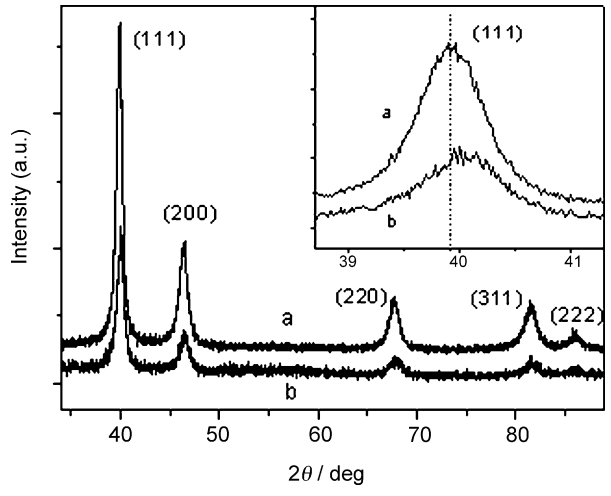

Fig. 3. XRD patterns of the electrodeposited Pt (a) and $Pt_{0.9}Pd_{0.1}$ alloy (b). The inset shows the magnification of the (1 1 1) peak region.

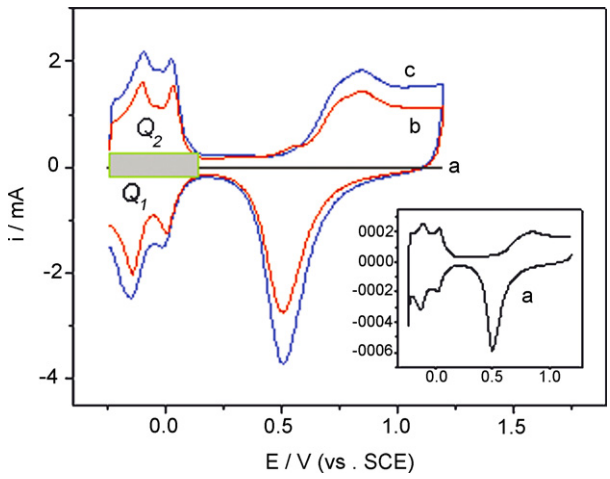

Fig. 4. CVs of Pt disc electrode (a), Pt/GCE (b) and $Pt_{0.9}Pd_{0.1}$/GCE (c) (the inset is the magnification of (a)). Solution: 1.0 M H_2SO_4. Scan rate: 100 mV s^{-1}. Q_1 and Q_2: the amount of charge for the electro-sorption and desorption of the H_2. The fill area is the contribution of double layer charge.

The calculated value of S from XRD method is roughly consistent with the electrochemically active surface area (EAS) [44], which can be measured by using hydrogen sorption and desorption peaks on the CV curves in 1.0 M H_2SO_4 solution. EAS can be expressed as

$$\mathrm{EAS} = 0.1\frac{Q_{\mathrm{ads}}}{Q_{\mathrm{ref}}L_{\mathrm{Pt}}} \tag{3}$$

where Q_{ads} is the integrated hydrogen absorption charge, Q_{ref} the hydrogen adsorption charge on a smooth platinum electrode (0.21 mC cm^{-2}) [38,39] and L_{Pt} is the Pt loading (mg).

Fig. 4 shows the CVs of the Pt disc electrode (a), Pt/GCE (b), and $Pt_{0.9}Pd_{0.1}$/GCE (c) in 1.0 M H_2SO_4 at 100 mV s^{-1}. The inset of Fig. 4 is the magnified image of the curve (a). Q_1 and Q_2 represent the amount of charge during the electro-sorption and desorption of the H_2 on the electrode surface and the filling area is the corresponding contribution of double layer charge. The coulombic charge for hydrogen adsorption (Q_{ads}) was used to calculate the EAS of catalysts. The value of the Q_{ads} was calculated as the mean value between the amounts of charge exchanged during the electro-sorption (Q_1) and desorption (Q_2) hydrogen on the modified electrode. A roughness factor was usually to express the ratio between the real surface area and the geometrical area of the electrode. From the area under the current–potential curve in the hydrogen region, the roughness factor was estimated to be much more than 560 and 790 times that of the well polished Pt disc electrode (Q_{ads} = 0.006 mC) for the Pt/GCE and $Pt_{0.9}Pd_{0.1}$/GCE, respectively. The significant enlargement of the surface area should be attributed to the CV-deposition procedure, which can result in deposition of nanostructured nano-clusters [45,46]. Table 3 summarizes the calculated values of d, Q_{ads}, EAS, L_{Pt} and the roughness factor of Pt/GCE and $Pt_{0.9}Pd_{0.1}$/GCE.

The enlarged effective surface area is benefit to enhance the catalytic activity of the prepared electrode. The MOR was tested at the Pt/GCE and $Pt_{0.9}Pd_{0.1}$/GCE. Fig. 5A shows CVs of MOR at $Pt_{0.9}Pd_{0.1}$/GCE (a) and Pt/GCE (b) in 1.0 M H_2SO_4 + 1.0 M

Table 3
Properties of the Pt/GCE and $Pt_{0.9}Pd_{0.1}$/GCE

Electrode	Q_1 (mC)	Q_2 (mC)	Q_{ads} (mC)	d (nm)	EAS ($m^2\,g^{-1}$)	L_{Pt} (mg)	Roughness factor
Pt/GCE	3.34	3.44	3.39	11.7	24.0	0.067	565
$Pt_{0.9}Pd_{0.1}$/GCE	4.77	4.69	4.73	10.1	28.6	0.079	

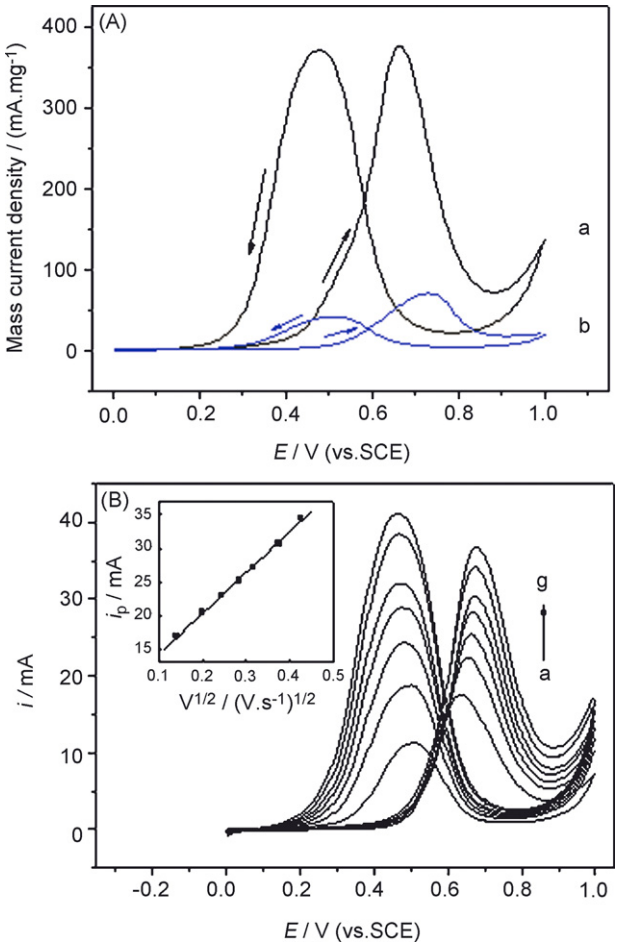

Fig. 5. CVs of MOR (A) at $Pt_{0.9}Pd_{0.1}$/GCE (a) and Pt/GCE (b) at a scan rate of 100 mV s^{-1}; (B) at $Pt_{0.9}Pd_{0.1}$/GCE at scan rates (a–g): 0.02–0.18 V/s (the inset is the forward anodic peak current vs. the square root of scan rate plot). Solution: 1.0 M H_2SO_4 + 1.0 M CH_3OH.

CH_3OH at a scan rate of 100 mV s^{-1}. MOR shows one anodic peak in the anodic scan and another in the reverse scan, which is normal [47]. On the reverse scan, the oxidation peak appeared at about 0.48 V and no reduction peak was observed. This is attributed to the adsorption and interaction of various intermediate species at the surface of the active sites of Pt [48]. Fig. 5(B) shows the CVs of methanol electro-oxidation at $Pt_{0.9}Pd_{0.1}$/GCE in 1.0 M CH_3OH + 1.0 M H_2SO_4 solution with different scan

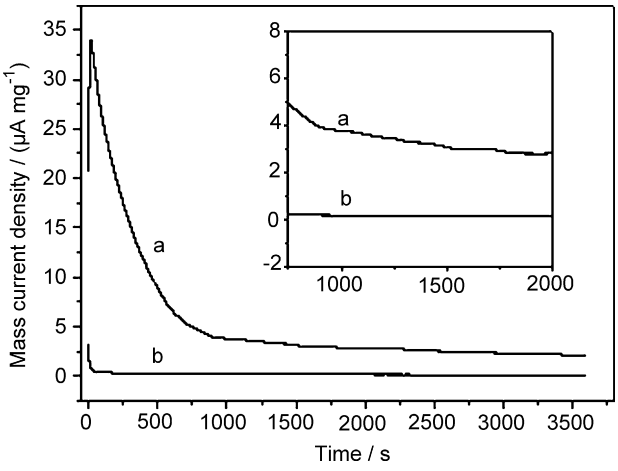

Fig. 6. Chronoamperometric curves at $Pt_{0.9}Pd_{0.1}$/GCE (a) and Pt/GCE (b) for MOR at 0.4 V in 1.0 M H_2SO_4 + 1.0 M CH_3OH.

rates (a–f: 0.04, 0.06, 0.08, 0.1, 0.12, 0.14 V s^{-1}). The result shows that the forward peak current is a linear function of the square root of the scan rate (the inset of Fig. 5B), indicating that methanol electro-oxidation was diffusion-controlled process. Results of MOR at different electrodes are listed in Table 4. Of all electrodes tested, $Pt_{0.9}Pd_{0.1}$/GCE shows both a greater negative shift of the onset oxidation potential and forward peak current potential, and a substantially greater mass current density, in comparison with those at Pt/GCE. The onset potential was estimated from the CV curve as the potential where the electrolysis current began to raise from the background charging current. Such a large enhanced catalytic activity for MOR can be attributed to the alloying, the "bifunctional catalysts" effect [49], and the nano-thickness porous structure in result of highly enlarged effective surface area. The role of Pd is a catalytically enhancing agent, which could modify the electronic properties of the Pt [50]. However, we also observed that the activity of the alloy greatly decreased if too much Pd is added into the alloy. This may be a result of over-dilution of the active sites of Pt.

To examine the long-term stability of $Pt_{0.9}Pd_{0.1}$/GCE in MOR, chronoamperometry tests in the solution was conducted for 3600 s as shown in Fig. 6. It shows that the initial mass current density is about 3 mA mg^{-1} at Pt/GCE (b), and it quickly decreases to about 1/5 of the initial value at about 20 s and almost disappears after 1000 s (the inset) at Pt/GCE (b). The initial mass

Table 4
Results for MOR at different electrodes

Electrode	Oriset of oxidation potential (mV)	Forward peak current potential (mV)	Mass peak current density (mA mg^{-1})
Pt/GCE	408	730	70
$Pt_{0.9}Pd_{0.1}$/GCE	213	664	7.6

current density is about 33 mA mg^{-1} at $Pt_{0.9}Pd_{0.1}$/GCE (a), and it decreases to about 1/5 at about 500 s, then, decreases slowly after 1000 s, but 2.4 mA mg^{-1} remains at 3500 s. The decrease of current density at both the electrodes is due to the surface poisoning from the intermediate species, such as CO_{ads}, CH_3OH_{ads}, and CHO_{adas} generated from MOR. The poisoning may be partially removed by potential cycling between 1.0 and −0.3 V at 100 mV s^{-1} for 10 cycles in 1.0 M H_2SO_4. It was found that about 65% of the initial mass current density can be regained for $Pt_{0.9}Pd_{0.1}$/GCE, but only 40% for Pt/GCE. These results show that the nanoporous $Pt_{0.9}Pd_{0.1}$ alloy film has better long-term stability, which is valuable for practical performance.

The excellent chronoamperometric behavior of $Pt_{0.9}Pd_{0.1}$/GCE cannot be simply attributed to the enhanced higher electrode surface area, but rather to the Pd alloying, which acts as a efficient catalytically enhancing agent, may also participate the methanol oxidation reaction through bifunctional mechanism.

The $Pt_{0.9}Pd_{0.1}$/GCE was exposed either in the air or immersed in 1.0 M H_2SO_4 solution for a month and negligible changes in the peak current and the peak potential for MOR were observed, indicating very good stability. In addition, the electrode is simple in preparation, and, probably more important, adaptable to ORR usage.

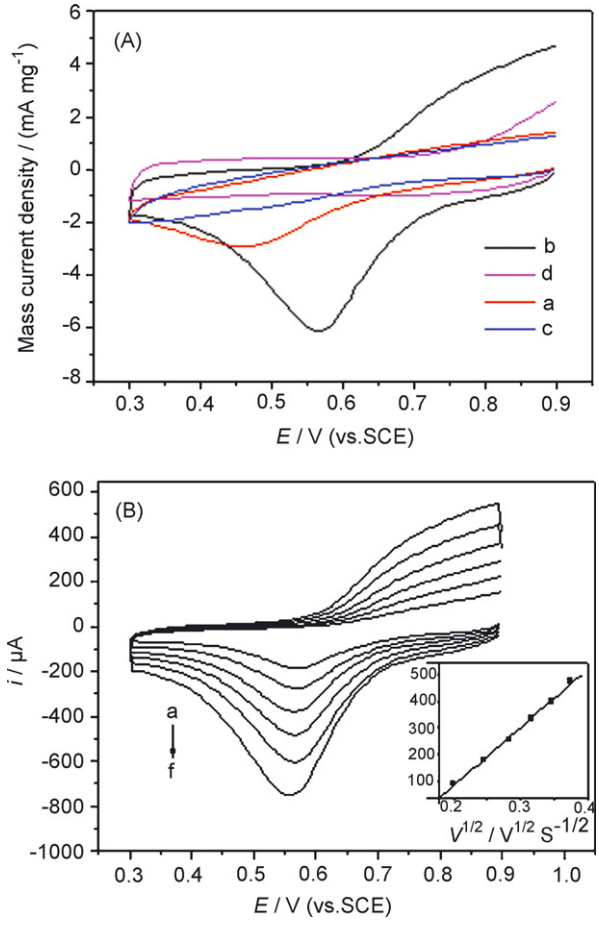

Fig. 7. (A) CVs of ORR at different electrodes: Pt/GCE (a), $Pt_{0.9}Pd_{0.1}$/GCE (b), in O_2-saturated 0.5 M H_2SO_4 solution and Pt/GCE (c), $Pt_{0.9}Pd_{0.1}$/GCE (d), in N_2-saturated 0.5 M H_2SO_4. Scan rate: 100 mV/s. (B) CVs of the ORR at $Pt_{0.9}Pd_{0.1}$/GCE in O_2-saturated 1.0 M H_2SO_4 with different scan rate (a–f): 0.04, 0.06, 0.08, 0.1, 0.12, 0.14 V s^{-1}. The inset of the (B) shows the plot of the peak currents of ORR vs. the square root of scan rate.

We found that the $Pt_{0.9}Pd_{0.1}$/GCE has also excellent catalytic ability toward ORR. Fig. 7A shows the CVs of ORR at Pt/GCE and $Pt_{0.9}Pd_{0.1}$/GCE in the O_2-saturated solution (a and b) in comparison with that in the N_2-saturated solution (c and d). In comparison with the ORR at Pt/GCE (a), the $Pt_{0.9}Pd_{0.1}$/GCE (b) shows much higher catalytic activity. The mass peak current density is about 2.5 times higher and the peak potential at 0.570 V is 100 mV lower. Fig. 7B shows the CVs of oxygen electro-reduction at $Pt_{0.9}/Pd_{0.1}$/GCE in O_2-saturated 1.0 M H_2SO_4 solution with different scan rates. The result showed that the peak currents is a linear function of the square root of scan rate (the inset of Fig. 7B), indicating that oxygen electro-reduction was diffusion-controlled process. In comparison with the other GCEs modified by either Pdnano/QDVP-Os/4-ABA hybrid film [51], Ptnano/CoTMPyP multilayer films [52], or Pt-coated gold nanoparticle monolayer film [53], our preparation method was very simple and our $Pt_{0.9}Pd_{0.1}$/GCE gives much higher surface area, >160 mV more positive ORR peak potential.

On the other hand, the mechanical strength of the $Pt_{0.9}Pd_{0.1}$/GCE was also tested by sonicating it in doubly distilled water for 5 min, and no change in the CV was observed.

4. Conclusion

Chemically and mechanically stable nano-thickness porous $Pt_{0.9}Pd_{0.1}$ alloy film modified GCE ($Pt_{0.9}Pd_{0.1}$/GCE) with 790-fold enhanced effective surface area than corresponding Pt disc electrode has been firstly generated by a very facile multi-cycle CV deposition on GCE. The Pt/Pd atomic ratio of 9:1 in the alloy was found optimal for MOR and ORR. The $Pt_{0.9}Pd_{0.1}$/GCE has significantly higher catalytic activity and stability for both ORR and MOR than similarly electrodeposited Pt modified GCE, demonstrating the Pd is an excellent catalytically enhancing agent for syntheses of effective platinum-based alloy catalyst in electrochemical applications. This $Pt_{0.9}Pd_{0.1}$/GCE and the CV-deposition method may have promising applications in biosensors and fuel cells, etc.

Acknowledgements

We gratefully acknowledge the support of this work by the National Natural Science Foundation of China (Grant No. 20575062) and the Specialized Research Fund for the Doctoral Program of Higher Education (Grant No. 20040358021).

References

[1] Y.L. Yao, Y. Ding, L.S. Ye, X.H. Xia, Carbon 44 (2006) 61.
[2] W.Z. Li, C.H. Liang, W.J. Zhou, J.S. Qiu, Z.H. Zhou, G.Q. Sun, Q. Xin, J. Phys. Chem. B 107 (2003) 6292.
[3] G.S. Attard, C.G. Goltner, J.M. Corker, S. Henke, R.H. Templer, Angew. Chem. Int. Ed. 36 (1997) 1315.
[4] H. Boo, S. Park, B.Y. Ku, Y. Kim, J.H. Park, H.C. Kim, T.D. Chung, J. Am. Chem. Soc. 126 (2004) 4524.
[5] P. Jiang, J.F. Bertone, V.L. Colvin, Science 291 (2001) 453.
[6] X.S. Peng, K. Koczkur, S. Nigro, A.C. Chen, Chem. Commun. (2004) 2872.

[7] J.F. Huang, I.W. Sun, Chem. Mater. 16 (2004) 1829.
[8] D.V. Pugh, A. Dursun, S.G. Corcoran, J. Electrochem. Soc. 152 (2005) B455.
[9] D.V. Pugh, A. Dursun, S.G. Corcoran, J. Mater. Res. 18 (2003) 216.
[10] M. Machida, K. Sato, I. Ishibashi, M. Abul Hasnat, K. Ikeue, Chem. Commun. (2006) 732.
[11] S. Koutsopoulos, S.B. Rasmussen, K.M. Eriksen, R. Fehrmann, Catal. Appl. A: Gen. 306 (2006) 142.
[12] Y.G. Wang, N. Shah, G.P. Huffman, Energy Fuel 18 (2004) 1429.
[13] S.M.A. Shibli, K.S. Beenakumari, Electroanalysis 18 (2006) 465.
[14] H. Tang, J.H. Chen, S.Z. Yao, L.H. Nie, G.H. Deng, Y.F. Kuang, Anal. Biochem. 331 (2004) 89.
[15] S.Q. Wang, L.P. Lu, X.Q. Lin, Electroanalysis 16 (2004) 1734.
[16] H.F. Cui, J.S. Ye, W.D. Zhang, J. Wang, F.S. Sheu, J. Electroanal. Chem. 577 (2005) 295.
[17] M. Pan, H.L. Tang, S.P. Jiang, Z.C. Liu, J. Electrochem. Soc. 152 (2005) A1081.
[18] H. Yang, C. Coutanceau, J.M. Leger, N. Alonso-Vante, C. Lamy, J. Electroanal. Chem. 576 (2005) 305.
[19] B. Rajesh, K.R. Thampi, J.M. Bonard, H.J. Mathieu, N. Xanthopoulos, B. Viswanathan, Electrochem. Solid State 7 (2004) A404.
[20] W. Huang, Z.L. Li, Y.D. Peng, Z.J. Niu, Chem. Commun. (2004) 1380.
[21] B.C. Beard, P.N. Ross, J. Electrochem. Soc. 137 (1990) 3368.
[22] E. Antolini, R.R. Passos, E.A. Ticianelli, Electrochim. Acta 48 (2002) 263.
[23] J.F. Drillet, A. Ee, J. Friedemann, R. Kotz, B. Schnyder, V.M. Schmidt, Electrochim. Acta 47 (2002) 1983.
[24] K. Ono, R. Okuda, Y. Ishii, S. Kamimura, M. Oshima, J. Phys. Chem. B 107 (2003) 1941.
[25] A.K. Shukla, R.K. Raman, N.A. Choudhury, K.R. Priolkar, P.R. Sarode, S. Emura, R. Kumashiro, J. Electroanal. Chem. 563 (2004) 181.
[26] H. Yang, N. Alonso-Vante, J.M. Leger, C. Lamy, J. Phys. Chem. B 108 (2004) 1938.
[27] J. Solla-Gullon, V. Montiel, A. Aldaz, J. Clavilier, Electrochem. Commun. 4 (2002) 716.
[28] S. Koutsopoulos, T. Johannessen, K.M. Eriksen, R. Fehrmann, J. Catal. 238 (2006) 206.
[29] Z.L. Liu, X.Y. Ling, X.D. Su, J.Y. Lee, J. Phys. Chem. B 108 (2004) 8234.
[30] N. Lewis, K. Topudurti, G. Welshans, R. Foster, J. Air Waste Manage. 40 (1990) 540.
[31] W.D. Bellamy, G.T. Hickman, P.A. Mueller, N. Ziemba, J. Water Pollut. Control Fed. 63 (1991) 120.
[32] Z.M. Qiang, J.H. Chang, C.P. Huang, Water Res. 36 (2002) 85.
[33] Z.Y. Wu, L.G. Chen, G.L. Shen, R.Q. Yu, Sens. Actuators B: Chem. 119 (2006) 295.
[34] N.M. Markovic, R.R. Adzic, B.D. Cahan, E.B. Yeager, J. Electroanal. Chem. 377 (1994) 249.
[35] S. Mukerjee, S. Srinivasan, M.P. Soriaga, J. Mcbreen, J. Electrochem. Soc. 142 (1995) 1409.
[36] S. Mukerjee, S. Srinivasan, M.P. Soriaga, J. Mcbreen, J. Phys. Chem. 99 (1995) 4577.
[37] T. Toda, H. Igarashi, H. Uchida, M. Watanabe, J. Electrochem. Soc. 146 (1999) 3750.
[38] S. Trasatti, O.A. Petrii, Pure. Appl. Chem. 63 (1991) 711.
[39] Z.L. Liu, J.Y. Lee, M. Han, W.X. Chen, L.M. Gan, J. Mater. Chem. 12 (2002) 2453.
[40] G. Liu, T.P. St. Clair, D.W. Goodman, J. Phys. Chem. B 103 (1999) 8578.
[41] N. Iwasa, N. Takezawa, Top. Catal. 22 (2003) 215.
[42] A.S. Arico, P.L. Antonucci, E. Modica, V. Baglio, H. Kim, V. Antonucci, Electrochim. Acta 47 (2002) 3723.
[43] Z.Q. Ma, P. Cheng, T.S. Zhao, J. Membr. Sci. 215 (2003) 327.
[44] A. Pozio, M. De Francesco, A. Cemmi, F. Cardellini, L. Giorgi, J. Power Sources 105 (2002) 13.
[45] S.Q. Wang, Y.M. Yin, X.Q. Lin, Electrochem. Commun. 6 (2004) 259.
[46] X.Q. Lin, Y.X. Li, Biosens. Bioelectron. 22 (2006) 253.
[47] W.J. Zhou, S.Q. Song, W.Z. Li, G.Q. Sun, Q. Xin, S. Kontou, K. Poulianitis, P. Tsiakaras, Solid State Ionics 175 (2004) 797.
[48] R. Parsons, T. Vandernoot, J. Electroanal. Chem. 257 (1988) 9.
[49] S. Motoo, M. Shibata, M. Watanabe, J. Electroanal. Chem. 110 (1980) 103.
[50] M.M.P. Janssen, J. Moolhuysen, Electrochim. Acta 21 (1976) 869.
[51] J.Y. Liu, L. Cheng, Y.H. Song, B.F. Liu, S.J. Dong, Langmuir 17 (2001) 6747.
[52] Y. Shen, J.Y. Liu, A.G. Wu, J.G. Jiang, L.H. Bi, B.F. Liu, Z. Li, S.J. Dong, Langmuir 19 (2003) 5397.
[53] Y.D. Jin, Y. Shen, S.J. Dong, J. Phys. Chem. B 108 (2004) 8142.